This manuscript has been published by the Journal of Constructional Steel Research 2019, Vol. 153: 330-342
DOI: doi.org/10.1016/j.jcsr.2018.10.026

Generalised Component Model for Structural Steel Joints

Chen Zhu[1], Kim J. R. Rasmussen[2], Shen Yan[3]

[1] PhD student, School of Civil Engineering, University of Sydney, Sydney NSW 2006, Australia. E-mail: czhu7452@uni.sydney.edu.au

[2] Professor, School of Civil Engineering, University of Sydney, Sydney NS 2006, Australia. E-mail: kim.rasmussen@sydney.edu.au

[3] Post-doctoral Fellow, School of Civil Engineering, University of Sydney, Sydney NSW 2006, Australis. E-mail: shen.yan@sydney.edu.au

Abstract: This paper presents a generalised component model for structural steel joints that extends the Component Method to the post-ultimate and post-fracture ranges. In this approach, a tri-linear spring model was developed for each individual component to include their post-ultimate behaviour, and a new concept of the instantaneous centre of rotation was introduced to track the changing load condition of each series of springs in a multi-spring system. The proposed generalised component model can predict the full-range M - θ curves of multi-spring models containing any number of deformable springs, and does not pose numerical difficulties in the post-ultimate range where some springs unload. The method is potentially applicable to all types of steel joints. The paper presents the application of the method to recent experimental tests on bolted moment end plate connections, showing good agreement over the full range of behaviour including fracture. The paper also

This manuscript has been published by the Journal of Constructional Steel Research 2019, Vol. 153: 330-342
DOI: doi.org/10.1016/j.jcsr.2018.10.026

demonstrates the application of the method to produce the backbone curve for a hysteretic model for the bolted moment end-plate connection.

Key words: component method; post-ultimate behaviour; post-fracture behaviour; end-plate connection; backbone curve.

1. Introduction

It is common practice in conventional design of structural steel joints to simplify the behaviour into one of two extreme cases [1]: ideally pinned (flexible) and fully rigid. An ideally pinned joint is free to rotate and therefore transmits no bending moment between the connected members, whereas a fully rigid joint provides full compatibility in rotation and transfers bending moments between connected members. However, real joints do not behave like these two extreme cases and therefore should be treated as "semi-rigid" [2], where bending moments are transferred and some relative rotation develops between connected members. For example, an angle cleat connection is usually assumed to be pinned but, in actuality, it can resist some bending moment and the design beam dimensions may decrease due to moment redistribution. Similarly, an extended end-plate joint classified as a rigid joint may adversely affect some members if a loss of rigidity in the "rigid" construction of the joint occurs. This discrepancy may result in a joint that is either ineffective or unsafe. Therefore, its semi-rigid behaviour must be assessed to improve its robustness.

The behaviour of a semi-rigid joint can be represented by a moment-rotation (M - θ) curve. The Component Method considers structural steel joints as a multi-spring model containing several parallel spring series, whereby the M - θ relationship of a structural steel joints can be obtained. The Method is currently used in Eurocode3 [3]. The Component Method specified in the early versions of Eurocode 3 could only predict a linear M - θ curve and did not include inelastic behaviour. Cleary, the linear curve does not cover many important characteristics and is insufficient for structural analysis of many practical joints. To overcome this limitation, Weynand et al. [4] proposed an additional empirical expression to represent the nonlinear post-yield joint behaviour, and this empirical expression is adopted in the current version of Eurocode3.

A theoretical method was developed in the early 2000s by da Silva and co-workers [5-7], in which a preloaded spring was added to the usual elastic spring to simulate yielding behaviour. While presenting a significant enhancement of the linear Component Method, the method had two limitations. Firstly, the complexity of the equations increased considerably with the number of springs and the complexity of the behaviour of each individual spring. Hence, a bi-linear spring was recommended in the method which did not allow for gradually yielding behaviour of the spring, nor the prediction of post-ultimate behaviour. Both of these ranges are important for predicting the final joint deformation and calculating the total energy absorbed by the joint. Secondly, the loading condition (tension or compression) of each spring was assumed in advance. However, the loading condition may change as the joint deforms, especially during the post-ultimate stage in which some of the springs have negative stiffness.

Building on the work of da Silva and co-workers, this paper outlines an approach referred to as the Generalised Component Method that uses a multi-spring system to characterise the joint behaviour including the post-ultimate and post-fracture effects. A tri-linear spring model is developed for each individual component to include their post-ultimate behaviour, and the concept of the instantaneous centre of rotation is introduced to track the changing loading condition of each series of springs in a multi-spring system. Moreover, an energy-based method is developed to extend the prediction of joint behaviour to the post-fracture range. Based on these enhancements, the proposed Generalised Component Method can predict the full-range M - θ curve of a multi-spring model containing any number of longitudinal deformable springs. This paper also presents examples of its application and validation against experimental tests. The generalised method is especially relevant seeing the ongoing development of procedures for designing structures by advanced analysis, referred to as the Direct Design Method [8], which requires the full-range behaviour of connections to be implemented for the analysis to accurately model

the behaviour and strength of connections, and their influence on load transfer between members. The Generalised Component Method can also be used to determine the backbone curve for seismic applications, as also demonstrated in this paper.

2. Energy-based formulation for an individual spring

Based on da Silva's work [5], a spring with bi-linear behaviour can be disassembled into two springs with linear behaviour, as shown in Fig. 1, including an elastic spring and a plastic spring. Although both springs behave linearly, the characteristics of their behaviours are different. The elastic spring is an ordinary spring whose F - Δ curve starts from the origin point and is always active under any load. On the contrary, the plastic spring is preloaded and does not deform until the applied force, F, reaches the critical load of activation, $P_{\mathrm{p}}^{\mathrm{C}}$. After activation of the plastic spring, along with the elastic spring, the plastic behaviour of the original spring can be reproduced.

The potential energy of the elastic spring in this dual-spring system (U_{e}) is written as:

$$U_{\mathrm{e}}=\frac{1}{2}k_{\mathrm{e}}\left(\Delta_{\mathrm{t}}-\left\langle\Delta_{\mathrm{p}}\right\rangle\right)^2 \tag{1}$$

where k_{e} is the stiffness of the elastic spring, Δ_{t} is the total displacement of the two-spring system, and Δ_{p} is the displacement of the plastic spring defined by:

$$\left\langle\Delta_{\mathrm{p}}\right\rangle\equiv\begin{cases}0, & F<P_{\mathrm{p}}^{\mathrm{C}}\\ \Delta_{\mathrm{p}}, & F\geq P_{\mathrm{p}}^{\mathrm{C}}\end{cases} \tag{2}$$

The potential energy of the plastic spring (U_{p}) can be written as:

$$U_{\mathrm{p}}=\frac{1}{2}k_{\mathrm{p}}\left(\frac{P_{\mathrm{p}}^{\mathrm{C}}}{k_{\mathrm{p}}}+\left\langle\Delta_{\mathrm{p}}\right\rangle\right)^2 \tag{3}$$

where k_{p} is the stiffness of the plastic spring. So the total potential energy of the two-spring system, U, is:

$$U=U_{\mathrm{e}}+U_{\mathrm{p}} \tag{4}$$

In this study, the post-ultimate behaviour of a spring is considered. To this end, the spring is disassembled into three springs, i.e., an elastic spring, a plastic spring and a softening spring, as shown in Fig. 2. The elastic spring and plastic spring are the same as those shown in Fig. 1, and the softening spring is used to reproduce the post-ultimate behaviour of the original spring. Similar to the plastic spring, the softening spring is also a preloaded spring. It does not deform until the applied force reaches the critical load of activation of the softening spring, $P_{\mathrm{s}}^{\mathrm{C}}$, which is also the ultimate capacity of the spring.

The energy equation for the elastic spring of this new spring series is modified to:

$$U_{\mathrm{e}}=\frac{1}{2}k_{\mathrm{e}}\left(\Delta_{\mathrm{t}}-\left\langle\Delta_{\mathrm{p}}\right\rangle-\left\langle\Delta_{\mathrm{s}}\right\rangle\right)^2 \tag{5}$$

where Δ_{s} is the displacement of the softening spring, defined by:

$$\left\langle\Delta_{\mathrm{s}}\right\rangle\equiv\begin{cases}0\,, & F<P_{\mathrm{s}}^{\mathrm{C}}\\ \Delta_{\mathrm{s}}\,, & F=P_{\mathrm{s}}^{\mathrm{C}}\ \text{and subsequent}\ F<P_{\mathrm{s}}^{\mathrm{C}}\end{cases} \tag{6}$$

The potential energy of a softening spring, U_{s}, can be obtained by subtracting the excessive energy from the total energy which is calculated by using the absolute value of its stiffness, k_{s}, as shown in Fig. 3:

$$U_{\mathrm{s}}=\frac{1}{2}\left|k_{\mathrm{s}}\right|\left(\frac{P_{\mathrm{s}}^{\mathrm{C}}}{\left|k_{\mathrm{s}}\right|}+\left\langle\Delta_{\mathrm{s}}\right\rangle\right)^2-\left|k_{\mathrm{s}}\right|\left\langle\Delta_{\mathrm{s}}\right\rangle^2 \tag{7}$$

Thus the total potential energy of the tri-linear spring is

$$U=U_{\mathrm{e}}+U_{\mathrm{p}}+U_{\mathrm{s}} \tag{8}$$

3. F - Δ behaviour of a spring series with post-ultimate behaviour

3.1 Energy equation of a spring series

Consider a spring series with n tri-linear springs (Fig. 4). The total energy of the spring series, Π, can be obtained from Eqs. (3), (5), (7) and (8):

$$\Pi=\frac{1}{2}k_{\mathrm{e,eq}}\left(\Delta_{\mathrm{t}}-\sum_{i=1}^{n}\left\langle\Delta_{\mathrm{p},i}\right\rangle-\sum_{i=1}^{n}\left\langle\Delta_{\mathrm{s},i}\right\rangle\right)^{2}+\sum_{i=1}^{n}\frac{1}{2}k_{\mathrm{p},i}\left(\frac{P_{\mathrm{p},i}^{\mathrm{C}}}{k_{\mathrm{p},i}}+\left\langle\Delta_{\mathrm{p},i}\right\rangle\right)^{2}+\sum_{i=1}^{n}\left[\frac{1}{2}\left|k_{\mathrm{s},i}\right|\left(\frac{P_{\mathrm{s},i}^{\mathrm{C}}}{\left|k_{\mathrm{s},i}\right|}+\left\langle\Delta_{\mathrm{s},i}\right\rangle\right)^{2}-\left|k_{\mathrm{s},i}\right|\left\langle\Delta_{\mathrm{s},i}\right\rangle^{2}\right]-F\Delta_{\mathrm{t}} \tag{9}$$

where $k_{\mathrm{e,eq}}$ is the equivalent stiffness of all the elastic springs, (since elastic springs are active at all times, they can be treated as a single equivalent spring), and can be calculated from the stiffness of each elastic spring i, $k_{\mathrm{e},i}$, by Eq. (10); the subscript i on the terms $\Delta_{\mathrm{p},i}$, $k_{\mathrm{p},i}$ and $P_{\mathrm{p},i}^{\mathrm{C}}$ represents the ith plastic spring; the subscript i on the terms $\Delta_{\mathrm{s},i}$, $k_{\mathrm{s},i}$ and $P_{\mathrm{s},i}^{\mathrm{C}}$ represent the ith softening spring.

$$\frac{1}{k_{\mathrm{e,eq}}}=\sum_{i=1}^{n}\frac{1}{k_{\mathrm{e},i}} \tag{10}$$

Assuming that $P_{\mathrm{p},1}^{\mathrm{C}}<P_{\mathrm{p},2}^{\mathrm{C}}<\cdots<P_{\mathrm{p,m-1}}^{\mathrm{C}}<P_{\mathrm{p,m}}^{\mathrm{C}}<P_{\mathrm{s,s}}^{\mathrm{C}}<\ldots$, the first plastic spring will be activated when the applied force reaches $P_{\mathrm{p},1}^{\mathrm{C}}$. As the applied force increases, other plastic springs will be activated one after the other until the plastic spring m is activated. Under increasing loading, the applied force eventually reaches the critical load of the softening spring with the smallest critical load, $P_{\mathrm{s},1}^{\mathrm{C}}$. From this point onwards, the resistance of this softening spring reduces as the total displacement keeps increasing, resulting in a reduction of the resistance of the entire spring series as well. Therefore, the plastic springs and the softening springs with critical loads larger than $P_{\mathrm{s},1}^{\mathrm{C}}$ will never be activated, i.e., $\Delta_{\mathrm{p},m+1}=\cdots=\Delta_{\mathrm{p},n}=\Delta_{\mathrm{s},2}=\cdots=\Delta_{\mathrm{s},n}=0$. The energy equation can be reduced to:

$$\Pi=\frac{1}{2}k_{\mathrm{e,eq}}\left(\Delta_{\mathrm{t}}-\sum_{i=1}^{m}\Delta_{\mathrm{p},i}-\Delta_{\mathrm{s},1}\right)^{2}+\sum_{i=1}^{m}\frac{1}{2}k_{\mathrm{p},i}\left(\frac{P_{\mathrm{p},i}^{\mathrm{C}}}{k_{\mathrm{p},i}}+\Delta_{\mathrm{p},i}\right)^{2}+\frac{1}{2}\left|k_{\mathrm{s},1}\right|\left(\frac{P_{\mathrm{s},1}^{\mathrm{C}}}{\left|k_{\mathrm{s},1}\right|}+\Delta_{\mathrm{s},1}\right)^{2}-\left|k_{\mathrm{s},1}\right|\left(\Delta_{\mathrm{s},1}\right)^{2}-F\Delta_{\mathrm{t}}+\Pi_{\mathrm{aux}} \tag{11}$$

$$\Pi_{\mathrm{aux}}=\sum_{i=m+1}^{n}\frac{1}{2}k_{\mathrm{p},i}\left(\frac{P_{\mathrm{p},i}^{\mathrm{C}}}{k_{\mathrm{p},i}}\right)^{2}+\sum_{i=2}^{n}\frac{1}{2}\left|k_{\mathrm{s},i}\right|\left(\frac{P_{\mathrm{s},i}^{\mathrm{C}}}{\left|k_{\mathrm{s},i}\right|}\right)^{2} \tag{12}$$

All activated springs other than the first softening spring will start to unload once $P_{\mathrm{s},1}^{\mathrm{C}}$ has been reached. Their unloading stiffness is equal to the elastic stiffness, and the plastic springs have no deformation during this process. Thus, the terms $\Delta_{\mathrm{p},1}$, …, $\Delta_{\mathrm{p},m-1}$ and $\Delta_{\mathrm{p},m}$ are constant once the first softening spring is activated.

3.2 Pre-ultimate stage of the F - Δ behaviour

For the pre-ultimate stage, the displacement of the first softening spring, $\Delta_{s,1}$, is zero. The energy equation (Eq. 11) becomes:

$$\Pi=\frac{1}{2}k_{e,eq}\left(\Delta_t-\sum_{i=1}^{m}\Delta_{p,i}\right)^2+\sum_{i=1}^{m}\frac{1}{2}k_{p,i}\left(\frac{P_{p,i}^C}{k_{p,i}}+\Delta_{p,i}\right)^2-F\Delta_t+\Pi_{aux} \tag{13}$$

where Π_{aux} is calculated from Eq. (12). Using the minimum total potential energy principle to find the springs' stationary position with respect to Δ_t, the force equilibrium equation for the equivalent elastic spring can be obtained:

$$\frac{\partial\Pi}{\partial\Delta_t}=k_{e,eq}\left(\Delta_t-\sum_{i=1}^{m}\Delta_{p,i}\right)-F=0 \tag{14}$$

Similarly, using the minimum total potential energy principle to find the springs' stationary positions with respect to $\Delta_{p,1}$, …, $\Delta_{p,m-1}$ and Δ_m, respectively, the force equilibrium equations for each individual plastic spring can be obtained:

$$\frac{\partial\Pi}{\partial\Delta_{p,ii}}=k_{e,eq}\left(\sum_{i=1}^{m}\Delta_{p,i}-\Delta_t\right)+k_{p,ii}\Delta_{p,ii}+P_{p,ii}^C=0 \qquad (ii=1,2,\cdots m) \tag{15}$$

All these equations contain a common term, i.e., $k_{e,eq}\left(\Delta_t-\sum_1^m\Delta_{p,i}\right)$. Thus:

$$F=k_{e,eq}\left(\Delta_t-\sum_{i=1}^{m}\Delta_{p,i}\right)=k_{p,1}\Delta_{p,1}+P_{p,1}^C=k_{p,2}\Delta_{p,2}+P_{p,2}^C=\cdots=k_{p,m-1}\Delta_{p,m-1}+P_{p,m-1}^C=k_{p,m}\Delta_{p,m}+P_{p,m}^C \tag{16}$$

This is the force equilibrium equation for the spring series where all the plastic spring forces are equal. Rearrange the terms in Eq. (16) to represent the displacement of each plastic spring in terms of $\Delta_{p,1}$:

$$\Delta_{p,ii}=\frac{k_{p,1}}{k_{p,ii}}\Delta_{p,1}+\frac{\left(P_{p,1}^C-P_{p,ii}^C\right)}{k_{p,ii}} \qquad (ii=1,2,\cdots m) \tag{17}$$

Add up $\Delta_{p,ii}$ and use the equation $k_{p,1}\Delta_{p,1}+P_{p,1}^C=F$ provided by Eq. (16), to obtain:

$$\sum_{i=1}^{m}\Delta_{p,i}=\left(\frac{1}{\langle K_{e/p}\rangle}-\frac{1}{k_{e,eq}}\right)F-\langle C_{e/p}\rangle \tag{18}$$

144 $$\left\langle K_{\mathrm{e/p}}\right\rangle \equiv \begin{cases} k_{\mathrm{e,eq}}, & F < P_{\mathrm{p,1}}^{\mathrm{C}} \\ \left(\dfrac{1}{k_{\mathrm{e,eq}}} + \displaystyle\sum_{i=1}^{m} \dfrac{1}{k_{\mathrm{p},i}}\right)^{-1}, & P_{\mathrm{p,1}}^{\mathrm{C}} \le F < P_{\mathrm{s,1}}^{\mathrm{C}} \end{cases} \tag{19}$$

145 $$\left\langle C_{\mathrm{e/p}}\right\rangle \equiv \begin{cases} 0, & F < P_{\mathrm{p,1}}^{\mathrm{C}} \\ \displaystyle\sum_{i=1}^{n} \dfrac{P_{\mathrm{p},i}^{\mathrm{C}}}{k_{\mathrm{p},i}}, & P_{\mathrm{p,1}}^{\mathrm{C}} \le F < P_{\mathrm{s,1}}^{\mathrm{C}} \end{cases} \tag{20}$$

146 where $\langle K_{\mathrm{e/p}}\rangle$ is the stiffness of the spring series in the elastic and/or plastic range and $\langle C_{\mathrm{e/p}}\rangle$ is the corresponding

147 preloading constant.

148 Substitute Eq. (18) into $F = k_{\mathrm{e,eq}}(\Delta_{\mathrm{t}} - \Sigma\Delta_{\mathrm{p},i})$ as in Eq. (16), to obtain:

149 $$F = \left\langle K_{\mathrm{e/p}}\right\rangle \left(\Delta_{\mathrm{t}} + \left\langle C_{\mathrm{e/p}}\right\rangle\right) \tag{21}$$

150 This is the pre-ultimate equation for the force-displacement relationship of a spring series consisting of n

151 springs and m activated plastic springs, where $\langle K_{\mathrm{e/p}}\rangle$ and $\langle C_{\mathrm{e/p}}\rangle$ are defined as per Eq. (19) and (20),

152 respectively.

153 3.3 Softening stage of the F - Δ behaviour

154 When the applied force just reaches $P_{\mathrm{s,1}}^{\mathrm{C}}$, based on Eq. (17), the plastic deformation of each individual plastic

155 spring can be obtained from:

156 $$P_{\mathrm{s,1}}^{\mathrm{C}} = k_{\mathrm{p},i}\Delta_{\mathrm{p},i} + P_{\mathrm{p},i}^{\mathrm{C}} \quad \left(i = 1, 2, \cdots, m\right) \tag{22}$$

157 Solve Eq. (22) for $\Delta_{\mathrm{p},i}$ and sum up all the plastic deformation terms:

158 $$\sum_{i=1}^{m} \Delta_{\mathrm{p},i} = \sum_{i=1}^{m} \frac{P_{\mathrm{s,1}}^{\mathrm{C}} - P_{\mathrm{p},i}^{\mathrm{C}}}{k_{\mathrm{p},i}} \tag{23}$$

159 Substituting Eq. (23) into Eq. (11), the total energy of the spring series becomes:

160 $$\Pi = \frac{1}{2} k_{\mathrm{e,eq}} \left(\Delta_{\mathrm{t}} - \sum_{i=1}^{m} \Delta_{\mathrm{p},i} - \Delta_{\mathrm{s,1}}\right)^2 + \frac{1}{2} \left|k_{\mathrm{s,1}}\right| \left(\frac{P_{\mathrm{s,1}}^{\mathrm{C}}}{\left|k_{\mathrm{s,1}}\right|} + \Delta_{\mathrm{s,1}}\right)^2 - \left|k_{\mathrm{s,1}}\right| \left(\Delta_{\mathrm{s,1}}\right)^2 - F\Delta_{\mathrm{t}} + \Pi_{\mathrm{aux}} \tag{24}$$

161 where

$$\Pi_{\text{aux}} = \sum_{i=1}^{m} \frac{1}{2} k_{\text{p},i} \left(\frac{P_{\text{p},i}^{\text{C}}}{k_{\text{p},i}} + \Delta_{\text{p},i} \right)^2 + \sum_{i=m+1}^{n} \frac{1}{2} k_{\text{p},i} \left(\frac{P_{\text{p},i}^{\text{C}}}{k_{\text{p},i}} \right)^2 + \sum_{i=2}^{n} \frac{1}{2} \left| k_{\text{s},i} \right| \left(\frac{P_{\text{s},i}^{\text{C}}}{\left| k_{\text{s},i} \right|} \right)^2 \tag{25}$$

Applying the minimum total potential energy principle to Eq. (24) with respect to Δ_{t} to find the stationary positions of the springs:

$$\frac{\partial \Pi}{\partial \Delta_{\text{t}}} = k_{\text{e,eq}} \left(\Delta_{\text{t}} - \Delta_{\text{s},1} - \sum_{i=1}^{m} \Delta_{\text{p},i} \right) - F = 0 \tag{26}$$

Similarly, applying the minimum total potential energy principle to Eq. (24) with respect to $\Delta_{\text{s},1}$ to find the stationary positions of the first softening spring:

$$\frac{\partial \Pi}{\partial \Delta_{\text{s},1}} = k_{\text{e,eq}} \left(\Delta_{\text{s},1} + \sum_{i=1}^{m} \Delta_{\text{p},i} - \Delta_{\text{t}} \right) - \left| k_{\text{s},1} \right| \Delta_{\text{s},1} + P_{\text{s},1}^{\text{C}} = 0 \tag{27}$$

Since $k_{\text{s},1} < 0$, $\left| k_{\text{s},1} \right| = -k_{\text{s},1}$. Thus combining Eq. (27) with Eq. (26) to obtain the force equilibrium equation:

$$F = k_{\text{e,eq}} \left(\Delta_{\text{t}} - \Delta_{\text{s},1} - \sum_{i=1}^{m} \Delta_{\text{p},i} \right) = k_{\text{s},1} \Delta_{\text{s},1} + P_{\text{s},1}^{\text{C}} \tag{28}$$

Extracting the force of the elastic springs and the force of the softening spring, an expression for $\Delta_{\text{s},1}$ in terms of Δ_{t} can be then obtained:

$$\Delta_{\text{s},1} = \left[k_{\text{e,eq}} \left(\Delta_{t} - \sum_{i=1}^{m} \Delta_{\text{p},i} \right) - P_{\text{s},1}^{\text{C}} \right] / \left(k_{\text{e,eq}} + k_{\text{s},1} \right) \tag{29}$$

Substituting Eq. (29) into Eq. (28), the softening-stage equation for the force-displacement relationship of spring series can be obtained:

$$F = K_{\text{s}} \left(\Delta_{\text{t}} + C_{\text{s}} \right) \tag{30}$$

$$\frac{1}{K_{\text{s}}} = \frac{1}{k_{\text{e,eq}}} + \frac{1}{k_{\text{s},1}} \tag{31}$$

$$C_{\text{s}} = \sum_{i=1}^{m} \frac{P_{\text{s},1}^{\text{C}} - P_{\text{p},i}^{\text{C}}}{k_{\text{p},i}} + \frac{P_{\text{s},1}^{\text{C}}}{k_{\text{s},1}} \tag{32}$$

where K_{s} is the stiffness of the spring series in the softening range and C_{s} is the corresponding preloading constant.

3.4 A unified formula

The force-displacement relationships set out above for the elastic, plastic and softening stages, i.e., Eq. (21) and Eq. (30), can be succinctly written as:

$$F = \left\langle K^j \right\rangle \left(\Delta_{\mathrm{t}} + \left\langle C^j \right\rangle \right) \tag{33}$$

$$\left\langle K^j \right\rangle \equiv \begin{cases} K_{\mathrm{e}}^j = \left(\sum_{i=1}^{n} \frac{1}{k_{\mathrm{e},i}} \right)^{-1}, & F < P_{\mathrm{p},1}^{\mathrm{C}} \\ K_{\mathrm{p}}^j = \left(\sum_{i=1}^{n} \frac{1}{k_{\mathrm{e},i}} + \sum_{i=1}^{m} \frac{1}{k_{\mathrm{p},i}} \right)^{-1}, & P_{\mathrm{p},1}^{\mathrm{C}} \le F < P_{\mathrm{s},1}^{\mathrm{C}} \\ K_{\mathrm{s}}^j = \left(\sum_{i=1}^{n} \frac{1}{k_{\mathrm{e},i}} + \frac{1}{k_{\mathrm{s},1}} \right)^{-1}, & F = P_{\mathrm{s},1}^{\mathrm{C}} \text{ and subsequent } F < P_{\mathrm{s},1}^{\mathrm{C}} \end{cases} \tag{34}$$

$$\left\langle C^j \right\rangle \equiv \begin{cases} C_{\mathrm{e}}^j = 0, & F < P_{\mathrm{p},1}^{\mathrm{C}} \\ C_{\mathrm{p}}^j = \sum_{i=1}^{m} \frac{P_{\mathrm{p},i}^{\mathrm{C}}}{k_{\mathrm{p},i}}, & P_{\mathrm{p},1}^{\mathrm{C}} \le F < P_{\mathrm{s},1}^{\mathrm{C}} \\ C_{\mathrm{s}}^j = \sum_{i=1}^{m} \frac{P_{\mathrm{s},1}^{\mathrm{C}} - P_{\mathrm{p},i}^{\mathrm{C}}}{k_{\mathrm{p},i}} + \frac{P_{\mathrm{s},1}^{\mathrm{C}}}{k_{\mathrm{s},1}}, & F = P_{\mathrm{s},1}^{\mathrm{C}} \text{ and subsequent } F < P_{\mathrm{s},1}^{\mathrm{C}} \end{cases} \tag{35}$$

where the superscript j on the terms K^j, K_{e}^j, K_{p}^j, K_{s}^j C^j, C_{e}^j, C_{p}^j and C_{s}^j represents different stiffness stages, the total number of which is denoted as N^j, as exemplified in Fig.5 for N^j=4.

4. M - θ behaviour of a multi-spring system

4.1 Energy equation for the multi-spring system

A multi-spring system with N parallel series of springs is now considered. Each series of springs may have a multi-linear F - Δ curve, which can be obtained by the method introduced in Section 3, and thus can be treated as a single spring with a multi-linear F - Δ behaviour, as shown in Fig. 6. The combined behaviour of the N parallel springs leads to a multi-linear moment-rotation (M - θ) curve, as shown in Fig. 7, where the superscript J = 1, 2,⋯,N^J represents the J^{th} segment of the M - θ curve, (the total number of segments N^J is chosen as 5 in

Fig. 7). In each segment, $M^J(\theta)$ is defined by unique matrixes of stiffness ($\boldsymbol{K}^J$) and preloading constant ($\boldsymbol{C}^J$). They contain the stiffness (K_I^j) and preloading constant (C_I^j) of each spring series I:

$$\boldsymbol{K}^J = \left[K_I^j \right]^J,\ I = (1, N) \text{ and } j \in \left(1, N_I^j\right) \tag{36}$$

$$\boldsymbol{C}^J = \left[C_I^j \right]^J,\ I = (1, N) \text{ and } j \in \left(1, N_I^j\right) \tag{37}$$

where N_I^j is the number of segments in the F - Δ curve of the Ith spring series. The spring series I may be either in the elastic ($K_I^j = K_{I,\mathrm{e}}^j$, $C_I^j = C_{I,\mathrm{e}}^j$), plastic ($K_I^j = K_{I,\mathrm{p}}^j$, $C_I^j = C_{I,\mathrm{p}}^j$) or post-ultimate range ($K_I^j = K_{I,\mathrm{s}}^j$, $C_I^j = C_{I,\mathrm{s}}^j$), as defined in Eqs. (34) and (35).

The energy expression for the system on the J^{th} linear curve of the multi-spring system can be written as:

$$\Pi^J = \sum_{I=1}^{N} \frac{1}{2} \left| K_I^j \right| a_I - M^J \theta \qquad \left(K_I^j \in \boldsymbol{K}^J \right) \tag{38}$$

$$a_I = \begin{cases} \left(\Delta_0 + h_I \sin\theta + C_{I,\mathrm{e}}^j \right)^2, & K_I^j = K_{I,\mathrm{e}}^j \\ \left(\Delta_0 + h_I \sin\theta + C_{I,\mathrm{p}}^j \right)^2, & K_I^j = K_{I,\mathrm{p}}^j \quad \left(C_I^j \in \boldsymbol{C}^J \right) \\ \left(\Delta_0 + h_I \sin\theta + \left| C_{I,\mathrm{s}}^j \right| \right)^2 - 2\left(\Delta_0 + h_I \sin\theta \right)^2, & K_I^j = K_{I,\mathrm{s}}^j \end{cases} \tag{39}$$

where Δ_0 is the displacement at the centroid of the connected beam, h_I is the height of spring series I measured from the centroid of the connected beam, and θ is the rotation of the joint, as shown in Fig. 8.

4.2 M - θ relation of the connection

Using the minimum total potential energy principle to find the system's stationary position, Eq. (38) is firstly differentiated with respect to Δ_0:

$$\frac{\partial \Pi^J}{\partial \Delta_0} = \sum_{I=1}^{N} \left| K_I^j \right| a_I' = 0 \qquad \left(K_I^j \in \boldsymbol{K}^J \right) \tag{40}$$

$$a_I' = \begin{cases} \Delta_0 + h_I \sin\theta + C_{I,\mathrm{e}}^j, & K_I^j = K_{I,\mathrm{e}}^j \\ \Delta_0 + h_I \sin\theta + C_{I,\mathrm{p}}^j, & K_I^j = K_{I,\mathrm{p}}^j \quad \left(C_I^j \in \boldsymbol{C}^J \right) \\ -\Delta_0 - h_I \sin\theta + \left| C_{I,\mathrm{s}}^j \right|, & K_I^j = K_{I,\mathrm{s}}^j \end{cases} \tag{41}$$

For the post-ultimate range, $\left| K_{I,\mathrm{s}}^j \right| = -K_{I,\mathrm{s}}^j$ and $\left| C_{I,\mathrm{s}}^j \right| = -C_{I,\mathrm{s}}^j$. Thus Eq. (40) and (41) can be simplified to:

$$\frac{\partial \Pi^J}{\partial \Delta_0} = \sum_{I=1}^{N} K_I^j \Delta_0 + \sum_{I=1}^{N} K_I^j h_I \sin\theta + \sum_{I=1}^{N} K_I^j C_I^j = 0 \tag{42}$$

from which $\Delta_0(\theta)$ can be obtained:

$$\Delta_0(\theta) = -\frac{\sum_1^N K_I^j h_I}{\sum_1^N K_I^j} \sin\theta - \frac{\sum_1^N K_I^j C_I^j}{\sum_1^N K_I^j} \tag{43}$$

Using again the minimum total potential energy principle, to obtain the M - θ relationship the total potential energy (Eq. (38)) is differentiated with respect to θ:

$$\frac{\partial \Pi^J}{\partial \theta} = \sum_{I=1}^{N} \left| K_I^j \right| a_I'' - M^J = 0 \qquad \left(K_I^j \in \boldsymbol{K}^J \right) \tag{44}$$

$$a_I'' = \begin{cases} \Delta_0 h_I \cos\theta + h_I^2 \sin\theta\cos\theta + C_{I,\mathrm{e}}^j h_I \cos\theta, & K_I^j = K_{I,\mathrm{e}}^j \\ \Delta_0 h_I \cos\theta + h_I^2 \sin\theta\cos\theta + C_{I,\mathrm{p}}^j h_I \cos\theta, & K_I^j = K_{I,\mathrm{p}}^j \quad (C_I^j \in \boldsymbol{C}^J) \\ -\Delta_0 h_I \cos\theta - h_I^2 \sin\theta\cos\theta + \left| C_{I,\mathrm{s}}^j \right| h_I \cos\theta, & K_I^j = K_{I,\mathrm{s}}^j \end{cases} \tag{45}$$

The above equations can be simplified utilising that in the post-ultimate range $\left|K_{I,\mathrm{s}}^j\right| = -K_{I,\mathrm{s}}^j$ and $\left|C_{I,\mathrm{s}}^j\right| = -C_{I,\mathrm{s}}^j$:

$$\frac{\partial \Pi^k}{\partial \theta} = \sum_{I=1}^{N} K_I^j \left(\Delta_0 h_I \cos\theta + h_I^2 \sin\theta\cos\theta + C_I^j h_I \cos\theta \right) - M^J = 0 \tag{46}$$

Then, substituting Eq. (43) for $\Delta_0(\theta)$ into Eq. (46), the expression for $M(\theta)$ can be obtained:

$$M(\theta) = -\frac{\left(\sum_1^N K_I^j h_I\right)^2}{\sum_1^N K_I^j} \sin\theta\cos\theta + \sum_{I=1}^{N} K_I^j h_I^2 \sin\theta\cos\theta + \sum_{I=1}^{N} K_I^j h_I C_I^j \cos\theta - \frac{\left(\sum_1^N K_I^j h_I\right)\left(\sum_1^N K_I^j C_I^j\right)}{\sum_1^N K_I^j} \cos\theta$$

(47)

Or, concisely:

$$M(\theta) = \left\{ \sum_{I=1}^{N-1} \sum_{II=I+1}^{N} K_I^j K_{II}^j \left(h_I - h_{II}\right) \left[\left(h_I - h_{II}\right) \sin\theta + \left(C_I^j - C_{II}^j\right) \right] \right\} \cos\theta \Big/ \sum_{I=1}^{N} K_I^j \tag{48}$$

5. Instantaneous centre of rotation (ICR)

In Eq. (48), although the F - Δ curves of all spring series are known, K_I^j and C_I^j are still undetermined because the loading condition (compression or tension, including unloading) of each individual spring series is unknown. Therefore, to determine K_I^j and C_I^j, the loading condition of a spring series must be obtained first. To this end, the concept of the instantaneous centre of rotation is utilised.

233 The instantaneous centre of rotation is defined as the point whose displacement is independent of section
234 rotation. The moving direction of any point on the rotating section can be determined by its position relative
235 position to this point, as demonstrated in Fig. 9. Assume the section rotates in the positive clockwise direction, if
236 a spring series is located above the ICR, it is under either tension or compressive unloading. Conversely, it is
237 under either compression or tensile loading if loaded below the ICR. Therefore, the loading condition of any
238 spring series can be analysed based on the moving direction of the section and its deformation history.

239 The displacement of a point on the rotating section can be represented by:

240 $$\Delta = \Delta_0 + h\sin\theta \tag{49}$$

241 where Δ is the displacement of a point on the rotating section and h is the height of this point measured from
242 the centroid of the connected beam, as shown in Fig. 8.

243 Substituting Eq. (43) into Eq. (49):

244 $$\Delta = \left(-\frac{\sum_1^N K_I^j h_I}{\sum_1^N K_I^j} + h \right) \sin\theta - \frac{\sum_1^N K_I^j C_I^j}{\sum_1^N K_I^j} \tag{50}$$

245 Since the displacement at the ICR is independent of the section rotation (θ), the bracketed term in Eq. (50)
246 must vanish and hence, the height and the displacement of the ICR can be derived as:

247 $$h_{\mathrm{ICR}} = \frac{\sum_1^N K_I^j h_I}{\sum_1^N K_I^j} \tag{51}$$

248 $$\Delta_{\mathrm{ICR}} = -\frac{\sum_1^N K_I^j C_I^j}{\sum_1^N K_I^j} \tag{52}$$

249 In the initial stage, $C_I^j = 0$, and therefore, $\Delta_{\mathrm{ICR}} = 0$, indicating the ICR and the zero displacement point
250 coincide and divide the tension and compression regions of the joint. Subsequently, when one or more of the
251 spring series yields, the stiffness and preloading constant of that spring series will change, and thus the height of
252 the ICR will change.

6. Post-fracture Behaviour

6.1 Energy-based method

In a multi-spring system, the fracture of a spring series may not lead to failure of the whole system because the rest of the system may sustain further rotation at lower resistance level. It is therefore of interest to consider the behaviour of a multi-spring system after the fracture of one or more of its spring series. It is here assumed that the ductility of each component spring is known, i.e., the force (F_f) and displacement (Δ_f) at fracture are known for each component, as shown in Fig. 2. Fracture of a component occurs when the displacement equals the fracture displacement, i.e., $\Delta = \Delta_f$, where $\Delta = \Delta_e + \Delta_p + \Delta_s$ can be obtained from $\Delta_e = F/k_e$, $\Delta_p = (F - P_p^C)/k_p$ and $\Delta_s = (F - P_s^C)/k_s$ according to Fig. 2.

The fracture of a spring series momentarily violates static equilibrium and induces dynamic effects, usually causing a sudden loss of resistance in the system. Since this study focuses on the static behaviour of the connection, how this dynamic behaviour affects the system is not addressed herein, and only the static equilibrium state of the system is studied.

An energy-based method is proposed to determine the new static equilibrium of the spring system, as shown in Fig. 10. After the fracture of a component, the new static equilibrium point should be located on the M - θ curve of the post-fracture multi-spring system, denoted by $M_{f,1}(\theta)$ in Fig. 10, where the spring series representing the fractured component is removed from the multi-spring system. Moreover, as the propagation of fracture in a component is usually unstable and thus very rapid, the potential energy possessed by the post-fracture system just after returning to static equilibrium, $V_{f,1}$, is assumed to equal the total energy possessed by the pre-fracture system at incipient component fracture, $V_{f,0}$. Successive fracture may occur in the remaining components

of the joint, causing loss of its resistance. Under such circumstance, this method can be repeated to obtain the entire post-fracture behaviour of the joint.

6.2 Application to the bolted moment end-plate connection

For bolted moment end-plate connections, one of the main components contributing to the joint rotation is the end-plate bending component. Bending of the end-plate causes severe deformation at the extended part of the end-plate, leading to crack initiation and propagation adjacent to the welds connecting the end-plate to the flange of the beam, as well as bolt fracture. Crack propagation and bolt fracture manifest themselves as stages of abrupt drops in bending moment resistance, as seen in recent tests reported by Zhu et al. [9]. Based on the experimental observations, three specific assumptions are made when applying the above energy-based method to end-plate connections.

Firstly, due to the random variations introduced during fabrication, the connection deformation and crack propagation are always found to be asymmetric to the vertical centreline of the end-plate. It is therefore assumed that fracture of a spring series is, in actuality, a two-step process. The stiffness and resistance of the spring series are therefore halved first, representing that fracture only occurs at one side of the component with the other side still being able to resist the applied load, and are subsequently reduced to zero indicating the failure of the whole component due to fracture.

Secondly, for other components than the end-plate, after fracture occurs, the stiffness is assumed equal to zero, i.e., the resistance of the post-fracture system is assumed to be constant during each post-fracture stage.

Thirdly, the connection is unstable in the post-fracture range; i.e., fracture propagation inside a component and among different components are consecutive. Thus, it is assumed that as soon as the system reaches the new static equilibrium point due to the fracture of a component, fracture occurs at the next potential component. The next

294 component to fracture is identified as the component which has the largest ratio Δ/Δ_f.This assumption may be
295 slightly conservative considering the experimental observation that the system may continue sustaining the same,
296 or even slightly higher, bending moment under increasing rotation.

297 Based on the above assumptions, the post-fracture model can be obtained using the following steps:

298 *a*. The component model detects a component fracture in a spring series at a connection rotation of $\theta_{f,0}$. This
299 is straightforward to do because the fracture point (Δ_f, F_f) of each component is assumed to be known.

300 *b*. Calculate the total energy of the multi-spring system model at $\theta_{f,0}$, $V_{f,0}(\theta_{f,0})$.

301 *c*. The stiffness and strength of the fractured spring series is reduced by 50% in the post-fracture system model.

302 *d*. Calculate the total energy of the new post-fracture system at $\theta_{f,0}$, $V_{f,1}(\theta_{f,0})$. It corresponds to the double-
303 hatched area shown in Figure 10.

304 *e*. The rotation of the new post-fracture system, $\theta_{f,1}$, can be calculated using Eq. (53) where $M_{f,1}(\theta_{f,0})$ is the
305 moment of the post-fracture system at $\theta_{f,0}$. Equation (53) is premised on the assumption that the potential energy
306 is preserved during fracture.

307 *f*. Repeat Steps *b* to *e* until all tension spring series have failed.

308 $$\theta_{f,1} = \frac{V_{f,0}(\theta_{f,0}) - V_{f,1}(\theta_{f,0})}{M_{f,1}(\theta_{f,0})} + \theta_{f,0} \quad (53)$$

309 ## 7 Model prediction and validation

310 The proposed generalized component model is first applied to the extended end-plate connection tests recently
311 reported in [9] for verification and validation purposes. Figure 11 presents an overview of the tested connections
312 which were under pure bending moment. All three connections were identical except for the thickness of the end-
313 plate and the back plate: connection S10 had a 10 mm thick end-plate but had no back plate; connection S10BP

had a 10 mm thick end-plate and a 20 mm thick back plate; connection S20BP had a 20 mm thick end-plate and a 20 mm thick back plate. The breakdown of the bolted moment end-plate connection into its individual components is visualized in Fig. 12, which illustrates the relevant components and the corresponding component model for the pure bending case. The corresponding components are (1) column web panel in shear, (2) column web in compression, (3) column web in tension, (4) column flange in bending (the back plate is considered as a part of the column flange), (5) end-plate in bending, and (10) bolts in tension.

By using the joint properties (actual material properties and dimensions reported in [9]), models for the individual components can be obtained. Linear models of the column web in tension and column web panel in shear components were obtained from Eurocode 3, Part 1.8. A full-range nonlinear model for the column web in compression component was obtained using the model presented in [10], which was simplified into a trilinear model considering the column web buckling and the post-ultimate ductile behaviour. Full-range models for the end-plate bending and column flange bending components were obtained using Swanson's T-stub model [11]. The bolts in tension components were considered collectively in the T-stub models. Each T-stub model was represented by a bi-linear model, where the resistance and stiffness were calculated based on corresponding effective widths obtained from Eurocode 3, Part 1.8, considering group effects. For the T-stub model, two failure modes were considered, namely, the weld fracture mode and the bolt fracture mode. The ultimate loads of these two failure models were determined as the nominal strength of the weld and the bolt, respectively. Tables 1 to 3 summarize the properties of each individual spring for the three connections.

Figures 13 to 15 show the model predictions and experimental results for the bending moment versus rotation response. The full-range behaviours of the connections, including the yielding and fracture of components, predicted by the proposed component model are in reasonable agreement with the experimental results. For

connection S20BP, the proposed component method shows that the bolts on the tensile side fracture one after another with no further connection rotation developed, and thus the post-fracture moment-rotation curve does not exhibit a stair-step shape. This is also consistent with the experimental observation that the fracture of the bolts at the outer bolt row significantly reduced the rotational ductility of the connection, leading to an instantaneous fracture of the bolts at the inner bolt row and complete collapse of the connection.

8. Backbone curve for hysteretic models

One of the many possible applications of the full-range M - θ model is in the earthquake field. In order to evaluate the seismic performance of a structural system, hysteretic models are required for the structural components of the system. The hysteretic model usually has a "backbone" curve and hysteresis rules that reproduce the cyclic loading behaviour of the component. The backbone curve is defined as the monotonic action-deformation curve of the structural component. Among other curves, according to Ibarra et al. [12], the backbone curve of a connection can be described as shown in Fig. 16, where K_e, α_s, α_c, λ, M_y, M_c, M_r, θ_y, θ_c, and θ_r are parameters of the backbone curve. In this section, the generalized component method developed herein is adopted to obtain the backbone curve for the hysteretic models of the extended end-plate connections tested in [9], i.e., connections S10, S10BP and S20BP.

The backbone curve also contains the negative bending moment part. By applying the generalised component model, the full-range joint behaviour with negative applied bending moment can be obtained. For connections S10, S10BP and S20BP, the full-range curves with both positive and negative moment are shown as the dash lines in Figs 17, 18 and 19, respectively. The entire backbone curve can be determined as an appropriate fit to the full-range curve. Table 4 summarizes the key parameters of the backbone curves.

9. Conclusions

This paper extends the Component Method to the post-ultimate range including fracture, and thus enables the full-range moment-rotation relationship of steel joints to be predicted. The method can be used to analyse spring models with any number of springs and does not pose numerical difficulties.

The enhancements made in this paper on the Component Method include: *a*. Equations for the F - Δ curve of a spring series with post-ultimate behaviour are derived. *b*. Equations for the M - θ curve of a multi-spring system, consisting of numerous parallel spring series including post-ultimate behaviour, are derived. *c*. The concept of the instantaneous centre of rotation is added to track the changing loading condition of each series of springs in a multi-spring system. *d*. An energy-based post-fracture model is presented to model the behaviour of the multi-spring system in the post-fracture range. The presented Generalised Component Method is potentially applicable to all types of joints, and has been applied to the bolted moment end-plate connection in this paper. As also demonstrated in this paper, the Method can be used to obtain the backbone curve for the hysteretic model of joints for seismic applications.

Acknowledgement

The work presented in this paper was funded by the Australian Research Council, Discovery project DP150104873.

Reference

[1] Hogan, T. J. Connection Design Guide 12 - Bolted end-plate to column moment connections. Australian Steel Institute Connection Design Guide, 2009.

[2] Wu, F. H. Semi-rigid connections in steel frames. Ph.D. Thesis, Purdue University, USA, 1988.

[3] CEN (European Committee for Standardization). EN 1993-1-8, Eurocode 3: design of steel structures, Part 1-8: design of joints. European Committee for Standardization, Brussels, 2010.

[4] Weynand, K., Jaspart, J. P., and Steenhuis, M. The stiffness model of revised annex J of Eurocode 3, in: R. Bjorhovde, A Colson, R Zandonini (Eds.), Connections in steel structures III. Proceedings of the 3rd Int.Workshop on Connections, 1996, Elsevier, Trento, 441–452.

[5] Simões da Silva, L., Girão Coelho, A. M., and Lucena Neto, E. Equivalent post-buckling models for the flexural behaviour of steel connections. Computers & Structures, 2000, 77, 615-624.

[6] Simões da Silva, L., and Girão Coelho, A. M. A ductility model for steel connections. Journal of Constructional Steel Research, 2001, 57, 45-70.

[7] Simões da Silva, L., Santiago, A., and Vila Real, P. Post-limit stiffness and ductility of end-plate beam-to-column steel joints. Computers & Structures, 2002, 80, 515-531.

[8] Rasmussen, K. J. R., and Zhang, H. Future challenges and developments in the design of steel structures – an Australian perspective. Proceedings of Eurosteel 2017, 2017, 1(2-3), 81-94.

[9] Zhu, C., Rasmussen, K. J. R., Yan, S., and Zhang, H. (2018). “Experimental Assessment of Bolted Moment End-plate Connections”. Journal of Structural Engineering. (Submitted).

[10] Zhu, C., and Rasmussen, K. J. R. Column Web Buckling Component Analysis. The International Colloquium on Stability and Ductility of Steel Structures, 2016, Timisoara, Romania, 1-9.

[11] Swanson, J. A., and Leon, R. T. Stiffness modeling of bolted T-stub connection components. Journal of Structural Engineering, 2001, 127, 498-505.

[12] Ibarra, L. F., Medina, R. A., and Krawinkler, H. Hysteretic models that incorporate strength and stiffness deterioration. Earthquake Engineering and Structural Dynamics, 2005, 34, 1489-1511.

396 **Nomenclature**

h_I	height of spring series I measured from the centroid of the connected beam
k_{e}	stiffness of elastic spring
$k_{\mathrm{e},i}$	stiffness of *i*th elastic spring
$k_{\mathrm{e,eq}}$	equivalent stiffness of all elastic springs
k_{p}	stiffness of plastic spring
$k_{\mathrm{p},i}$	stiffness of *i*th plastic spring
k_{s}	stiffness of softening spring
$k_{\mathrm{s},i}$	stiffness of *i*th softening spring

Capital letter

$C_{\mathrm{e/p}}$	preloading constant corresponding to $K_{\mathrm{e/p}}$
C_{s}	preloading constant corresponding to K_{s}
C_I^j	preload constant of the segment *j* of the spring series *I*
F	applied force on the spring series
$K_{\mathrm{e/p}}$	stiffness of the spring series in elastic and/or plastic range
K_{e}	elastic (initial) stiffness of backbone curve
K_{s}	stiffness of the spring series in softening range
K_I^j	stiffness of segment *j* of spring series *I*
M	applied moment on the connection
M_{y}	yield bending resistance of backbone curve

M_{c}	peak bending resistance of backbone curve
M_{r}	residual bending resistance of backbone curve
$P_{\mathrm{p}}^{\mathrm{C}}$	critical load of activation of plastic spring
$P_{\mathrm{p},i}^{\mathrm{C}}$	critical load of activation of *i*th plastic spring
$P_{\mathrm{s}}^{\mathrm{C}}$	critical load of activation of softening spring
$P_{\mathrm{s},i}^{\mathrm{C}}$	critical load of activation of *i*th softening spring
U_{e}	potential energy of the elastic springs in spring system
U_{p}	potential energy of the plastic springs in spring system
U_{s}	potential energy of the softening springs
U	total potential energy of the spring system
$V_{\mathrm{f},0}$	energy of pre-fracture system
$V_{\mathrm{f},1}$	energy of post-fracture system
Greek letters	
Δ_{p}	displacement of plastic spring
$\Delta_{\mathrm{p},i}$	displacement of *i*th plastic spring
Δ_{t}	total displacement of spring system
Δ_{s}	displacement of softening spring
$\Delta_{\mathrm{s},i}$	displacement of *i*th softening spring
Δ_0	displacement at the centroid of the connected beam
θ	rotation of joint
$\theta_{\mathrm{f},0}$	rotation of joint when fracture first occurs

$\theta_{f,1}$	rotation of joint when the system reaches new equilibrium
θ_y	yield rotation of backbone curve
θ_c	cap rotation of backbone curve
θ_r	residual rotation of backbone curve
α_s	strain-hardening stiffness parameter of backbone curve
α_c	post-capping stiffness parameter of backbone curve
λ	residual strength parameter of backbone curve
Π	total energy of spring system

397

Tables

Table 1. Component model parameters for connection S10.

Row	Component	h (m)	k_e (kN/m)	k_p (kN/m)	k_s (kN/m)	P_p^C (kN)	P_s^C (kN)
1	End-plate in bending	0.1935	440000	57800	-∞	220	389
	Column flange in Bending	0.1935	100000	6550	-∞	120	586
	Column web in tension	0.1935	879000	-	-	-	-
2	End-plate in bending	0.1035	629000	35900	-∞	440	586
	Column flange in bending	0.1035	100000	6550	-∞	120	586
	Column web in tension	0.1035	879000	-	-	-	-
3	Column web in compression	-0.1475	2230000	70100	-9030	670	979
	Column web penal in shear	-0.1475	961000	-	-	-	-

Table 2. Component model parameters for connection S10BP.

Row	Component	h (m)	k_e (kN/m)	k_p (kN/m)	k_s (kN/m)	P_p^C (kN)	P_s^C (kN)
1	End-plate in bending	0.1935	440000	57800	-∞	220	389
	Column flange in Bending	0.1935	114000	9540	-∞	160	586
	Column web in tension	0.1935	879000	-	-	-	-
2	End-plate in bending	0.1035	629000	35900	-∞	440	586
	Column flange in bending	0.1035	114000	9540	-∞	160	586
	Column web in tension	0.1035	879000	-	-	-	-
3	Column web in compression	-0.1475	2230000	70100	-9030	670	979
	Column web penal in shear	-0.1475	961000	-	-	-	-

406 Table 3. Component model parameters for connection S20BP.

Row	Component	h (m)	k_e (kN/m)	k_p (kN/m)	k_s (kN/m)	P_p^C (kN)	P_s^C (kN)
1	End-plate in bending	0.1935	607000	34500	-∞	455	589
	Column flange in Bending	0.1935	114000	9540	-∞	160	586
	Column web in tension	0.1935	879000	-	-	-	-
2	End-plate in bending	0.1035	928000	25000	-∞	452	586
	Column flange in bending	0.1035	114000	9540	-∞	160	586
	Column web in tension	0.1035	879000	-	-	-	-
3	Column web in compression	-0.1475	2230000	70100	-9030	670	979
	Column web penal in shear	-0.1475	961000	-	-	-	-

407

408 Table 4: Key parameters of the backbone curves for the end-plate connections tested in [9].

		M_y (kN·m)	M_c (kN·m)	M_r (kN·m)	θ_y (rad)	θ_c (rad)	θ_r (rad)	K_e (kN·m/rad)	a_s	a_c
S10	Positive	72.1	211	63.2	0.00716	0.144	0.272	10100	0.100	-0.115
	Negative	-29.9	-138	-69.3	-0.00664	-0.330	-0.390	4500	0.0742	-0.256
S10BP	Positive	96.6	215	65.0	0.00877	0.0950	0.178	11000	0.125	-0.164
	Negative	-39.8	-142	-71.4	-0.00806	-0.221	-0.260	4940	0.0976	-0.336
S20BP	Positive	96.5	290	224	0.00844	0.151	0.256	11400	0.119	-0.0547
	Negative	-39.8	-142	-71.3	-0.00774	-0.221	-0.255	5150	0.0933	-0.404

409

Figures

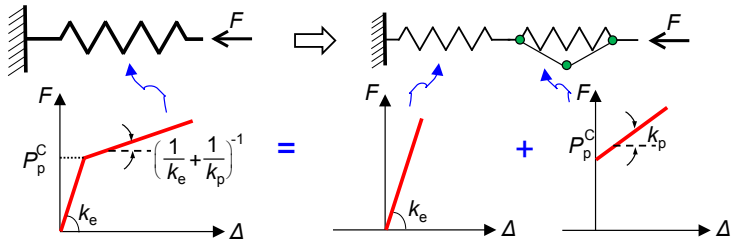

Figure 1. Use two linear springs to represent a bi-linear spring.

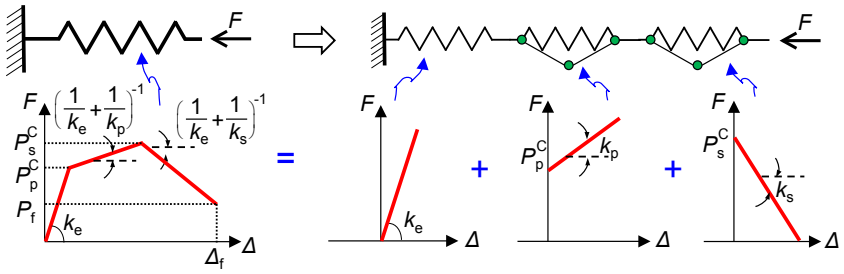

Figure 2. Use three springs to reproduce tri-linear behaviour of a spring.

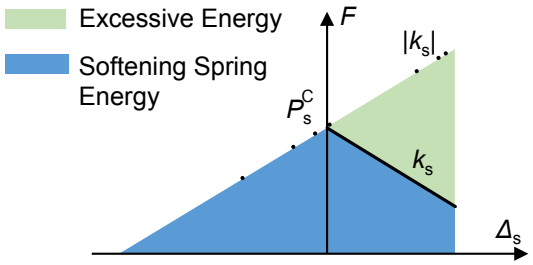

Fig. 3 Energy of a softening spring

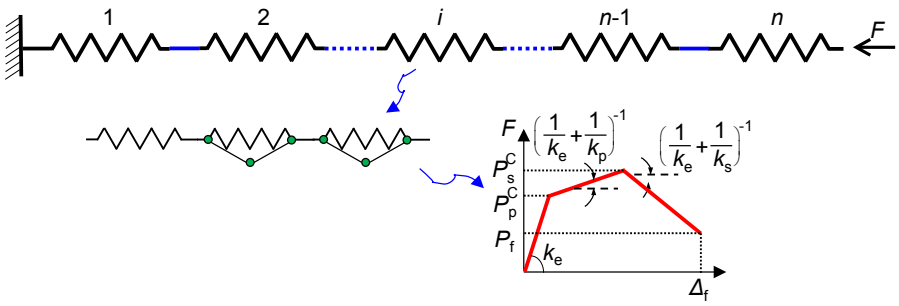

421

422 Figure 4. A series of n tri-linear springs.

423

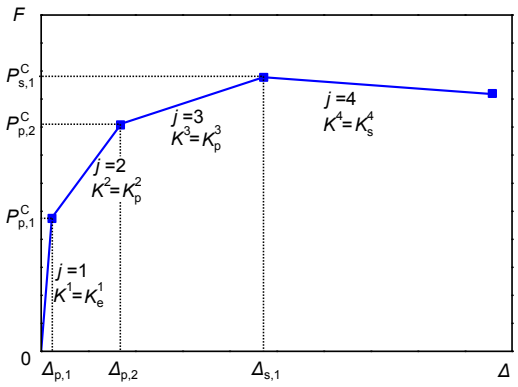

424

425 Figure 5. F - Δ curve of a spring series.

426

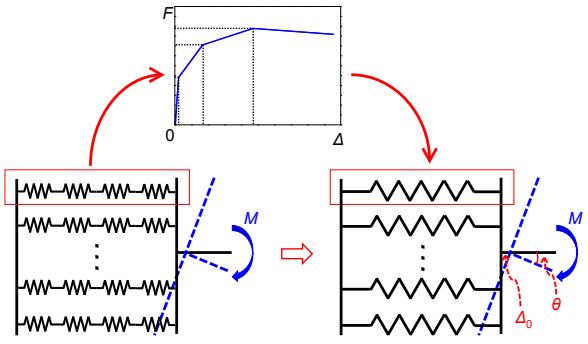

427

428 Figure 6. A multi-spring system.

429

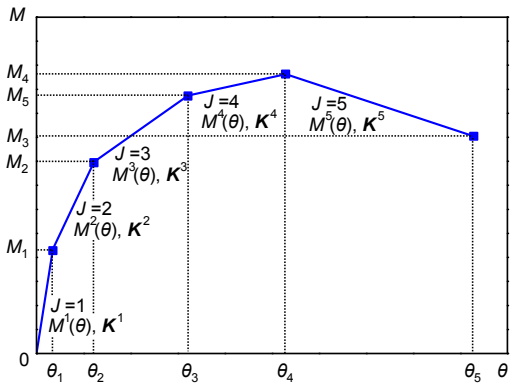

Figure 7. M - θ curve of a multi-spring system.

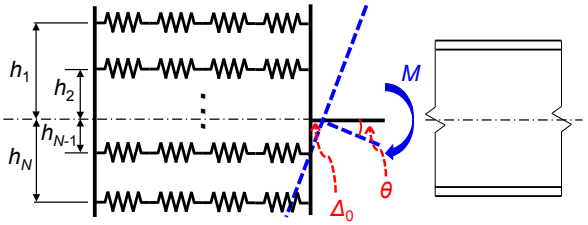

Figure 8. The height of each spring series in a multi-spring system.

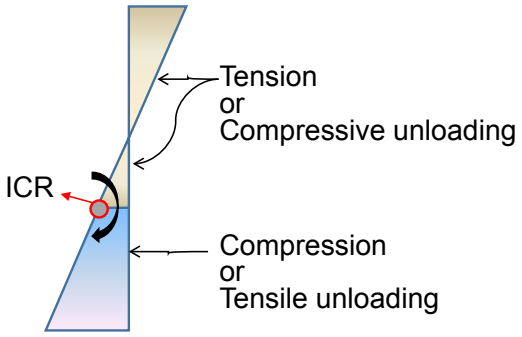

Figure 9. The concept of ICR and the loading condition of any point on a rotating section

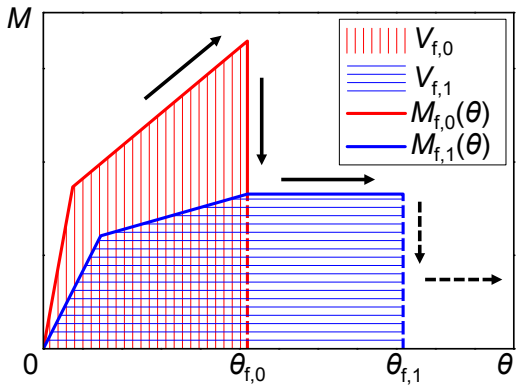

439

440 Figure 10. Energy method to obtain the post-fracture M - θ curve of a spring system.

441

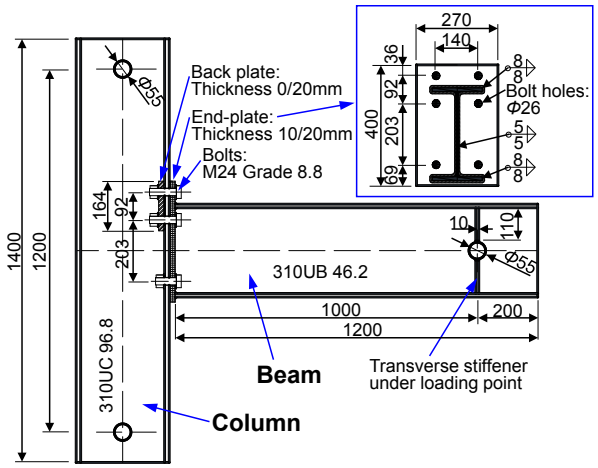

442

443 Fig. 11. Tested extended end-plate connection reported in [9].

444

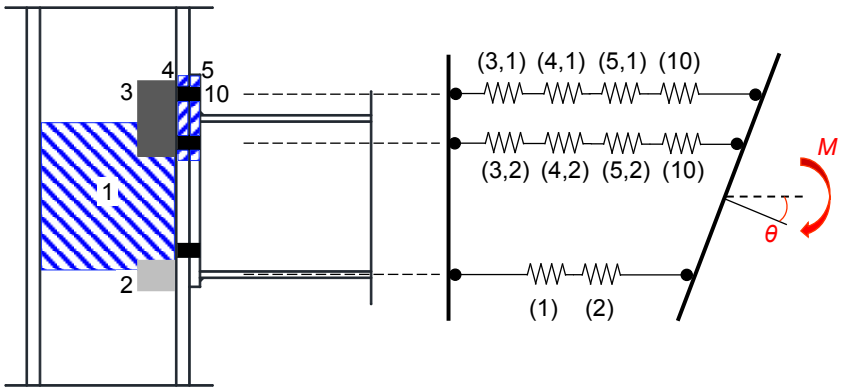

445

446 Figure 12. Component identification and corresponding component model for bending.

447

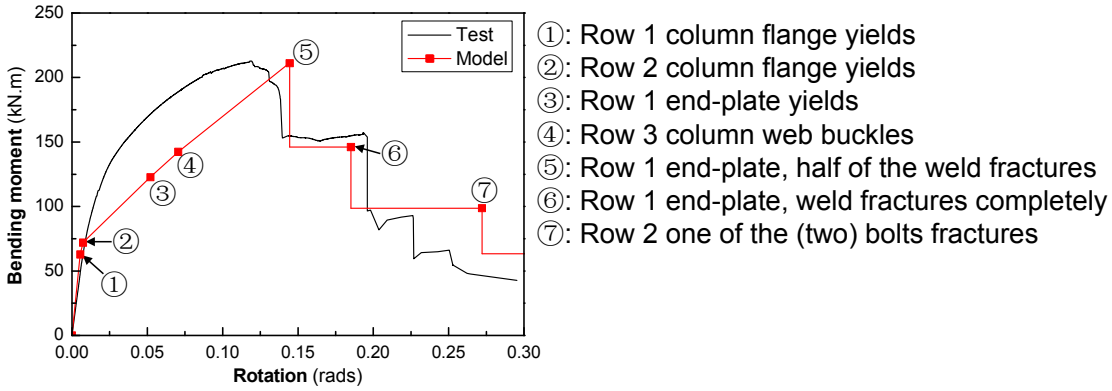

448

449 Figure 13. M - θ curve of S10 obtained by the component model and its comparison against the test result.

450

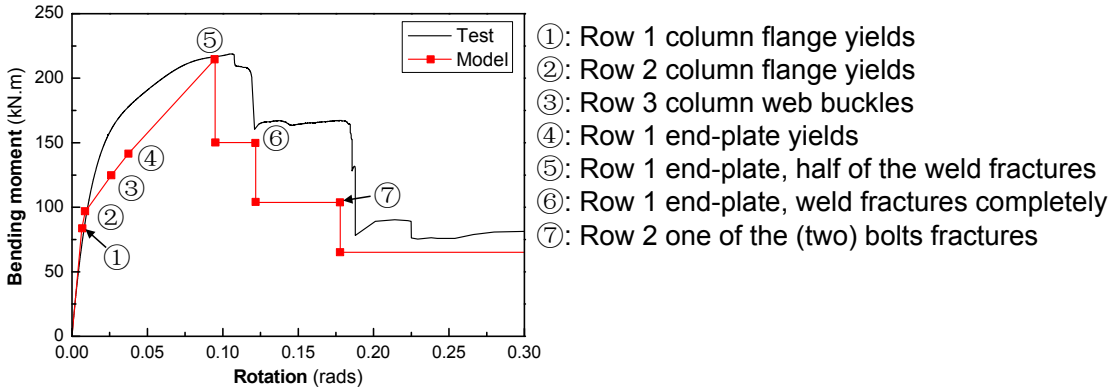

451

452 Figure 14. M - θ curve of S10BP obtained by the component model and its comparison against the test result.

453

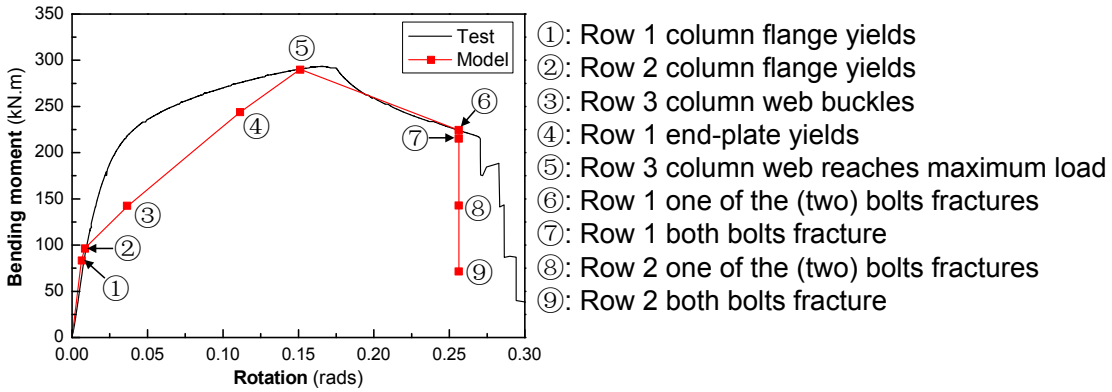

454

455 Figure 15. M - θ curve of S20BP obtained by the component model and its comparison against the test result.

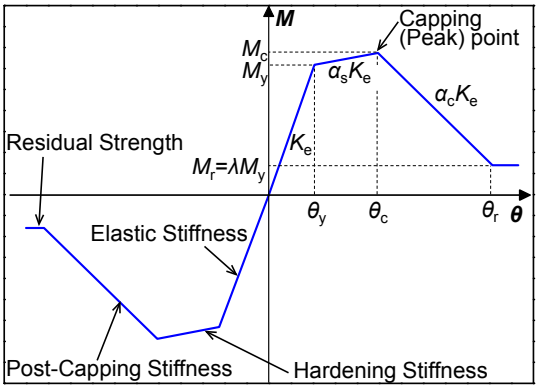

456

457 Figure 16. Backbone curve for hysteretic models of steel joints (redrawn from [12]).

458

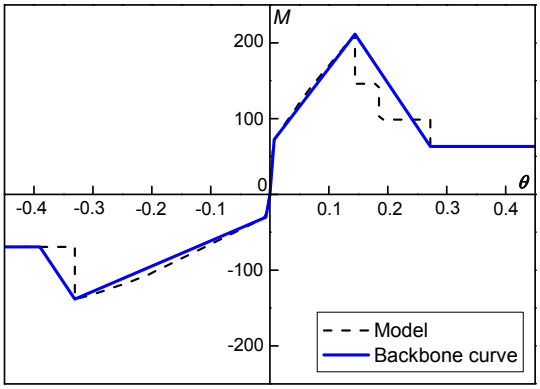

459

460 Figure 17. Backbone curve for the end-plate connection S10.

461

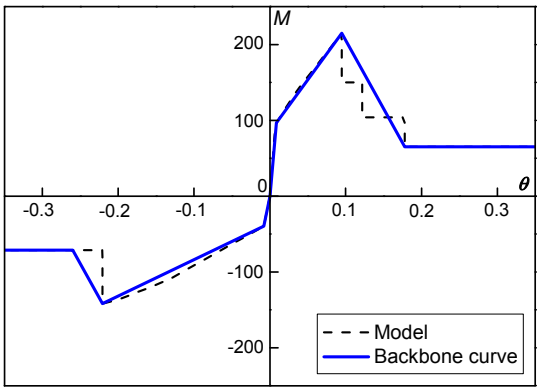

462

463 Figure 18. Backbone curve for the end-plate connection S10BP.

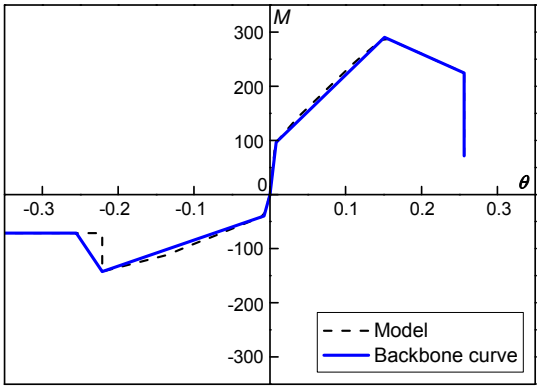

464

465 Figure 19. Backbone curve for the end-plate connection S20BP.